



Research article

A green approach to develop zeolite-thymol antimicrobial composites: analytical characterization and antimicrobial activity evaluation



Stefania Cometa^{a,1}, Maria A. Bonifacio^{b,c,1}, Annalisa Bellissimo^a, Loris Pinto^d, Andrea Petrella^e, Nicoletta De Vietro^b, Giuseppe Iannaccone^a, Federico Baruzzi^{d,**}, Elvira De Giglio^{b,c,*}

^a Jaber Innovation s.r.l., Via Calcutta 8, 00144, Rome, Italy

^b Department of Chemistry, University of Bari, Via Orabona 4, 70126, Bari, Italy

^c INSTM, National Consortium of Materials Science and Technology, Via G. Giusti 9, 50121, Florence Italy

^d Institute of Sciences of Food Production, National Research Council of Italy, Via G. Amendola 122/O, 70126, Bari, Italy

^e Department of Civil, Environmental, Land, Building Engineering and Chemistry, Polytechnic University of Bari, Via E. Orabona, 4, Bari, 70125, Italy

ARTICLE INFO

Keywords:

Zeolite
Thymol
Antimicrobial activity
Hybrid composite
Surface characterization
Solvent-free process

ABSTRACT

In this work, the development, analytical characterization and bioactivity of zeolite-thymol composites, obtained using wet, semi-dry and dry processes, were carried out in order to obtain sustainable and powerful antimicrobial additives. FT-IR, XRD, DSC, TGA, SEM and B.E.T. analyses were carried out to gain comprehensive information on the chemical-physical, thermal, and morphological features of the composites. GC-MS analyses allowed quantifying the active molecule loaded in the zeolite, released by the functionalized composites and its stability over time. Among the three procedures, the dry approach allowed to reach the highest thymol loading content and efficiency ($49.8 \pm 1.6\%$ and $99.6 \pm 1.2\%$, respectively), as well as the highest composite specific surface area value, feature which promises the best interaction between the surface of the composite and the bacterial population. Therefore, the bioactive surface of composites obtained by this solvent-free method was assayed for its antimicrobial activity against four microbial strains belonging to *Staphylococcus aureus*, *Escherichia coli*, *Pseudomonas aeruginosa* and *Candida albicans* species. The higher antimicrobial activity produced by the solvent-free composite in comparison with that of pure thymol, at the same thymol concentration, was ascribed to the large interfacial contact between the composite and the bacterial target. This feature, together with its enhanced storage stability, suggested that this composite could be employed as effective additives for the development of antimicrobial biointerfaces for food, home and personal care applications.

1. Introduction

The challenge posed by bacterial resistance to multiple antibiotics is a huge health problem [1]. On the other hand, the use of alternative antimicrobial systems often poses an issue related to the potential toxicity of these systems, especially if nanosized [2]. In this respect, many plant extracts have been tested worldwide as potential sources of novel antimicrobial compounds, as alternative tools for the treatment of infectious diseases or as agents able to promote food and cosmetic preservation [3]. In particular, essential oils (EOs) are mixtures of several molecules extracted from different plant structures or species, showing antibacterial, antifungal, antiviral, antiparasitic, antimicrobial,

anticancer, antiinflammatory, antioxidant or radical scavenging features [4, 5, 6, 7, 8]. On the other hand, these molecules are often highly unstable, not soluble in aqueous solutions, susceptible to oxidation, thermal degradation and/or rapid volatilization. Due to their poor stability and high costs, a protection of these molecules is often required, to guarantee their safety, effectiveness, bioavailability, stability and quality. In literature, most of the vehicle systems consist of polymeric micro- or nanoparticles [9, 10, 11, 12, 13], liposomes, colloids, coatings, and emulsions, by means of encapsulation, adsorption, or absorption, grafting, functionalization or coverage processes. Alternatively, caged or lamellar clay minerals have been proposed as vehicles of EOs for various applications such as food packaging, hygienic-sanitary, pharmaceutical, agricultural

* Corresponding author.

** Corresponding author.

E-mail addresses: federico.baruzzi@ispa.cnr.it (F. Baruzzi), elvira.degiglio@uniba.it (E. De Giglio).

¹ These authors equally contributed to the work.

applications among others [14, 15, 16]. Usually, clay/EOs hybrid materials are prepared by wet procedures [17, 18], often modifying the clays resorting to quaternary alkyl ammonium surfactants to create a lipophilic environment for a better adsorption of EOs compounds [19]. The main drawback by using solvents is related to the low encapsulation yields, complex procedures, and non-sustainable processes. Some recent works exploited the facile volatilization of EOs by adsorption/evaporation procedure [20]. Due to the volatile nature of EOs and their consequent rapid loss via evaporation, the choice of the best encapsulation procedure of EOs in a vehicle remains an open issue.

Among the EOs constituents, thymol, an antimicrobial phenolic monoterpene that is the main and less volatile component of red thyme oil [21], represents a very interesting molecule, with the advantage of low cost and simple handling, being in a solid crystalline form. For these reasons, thymol has already been included as active molecule in several EPA-approved disinfectants for use against SARS-CoV-2, to treat surfaces in healthcare, institutional or residential sites [22]. Although thymol represents one of the main active antifungal compounds for vapor phase applications [23], its use is limited by its low solubility in water.

Zeolites are tectosilicates of natural or synthetic origin, with an open lattice framework, containing silica and alumina tetrahedrons and forming molecular sized pores in a variety of dimensions and geometries useful for many sustainable processes [24]. Zeolites have been also used in combination with Ag, Cu or Zn ions [25], or subjected to organic functionalization via adsorption of quaternary ammonium compounds (QACs) [26], to produce antimicrobial systems. Recently, Dikić and co-workers [27] prepared a composite based on a natural zeolite (clinoptilolite) and carvacrol or thymol by supercritical solvent impregnation (SSI) in supercritical carbon dioxide (scCO₂). The composites showed antibacterial activity toward *Escherichia coli* and *Staphylococcus aureus* strains. Differently from the SSI process in scCO₂, that need specific and expensive equipment, here we propose simple and cost-effective methods to vehicle and protect thymol using a zeolite framework. In particular, three preparation methods of the zeolite/active agent composite were tested and compared, i.e., wet, semi-dry and dry or solvent-free process. Chemical-physical analyses, i.e., Fourier Transform Infrared Spectroscopy (FT-IR), X-ray diffraction (XRD), Differential Scanning Calorimetry (DSC), Thermo-Gravimetric Analysis (TGA), Scanning Electron Microscopy/Energy Dispersive X-ray (SEM/EDX), Brunauer, Emmett and Teller

(B.E.T.) specific surface area (SSA) and Gas Chromatography coupled with Mass Spectrometry (GC-MS) allowed to characterize the bioactive composites. The efficacy of the inorganic caged material against the rapid volatilization of the monoterpene was tested by storage performance tests. The dry process resulted the most convenient and straightforward method for the production of a zeolite-thymol hybrid composite, showing the most promising interfacial characteristics among the three studied procedures (i.e., small thymol crystallite sizes, low aggregation degree, high pore surface area and volume values). Therefore, microbiological assays of the dry formulation against different pathogens were carried out. In conclusion, among the three tested methods, the dry process resulted the most suitable method to achieve a zeolite-thymol hybrid composite endowed with antimicrobial activity.

2. Experimental

2.1. Materials

Thymol (2-isopropyl-5-methylphenol) (purity $\geq 98.5\%$) was purchased by *Sigma Aldrich* (Italy) and the Zeolite 4A (coded as ZEO4A, purity $>98\%$, D₅₀ 3.5 μm), having an interconnected 3D network of channels approximately 4 Å in diameter, in addition to larger "cages" approximately 7 Å in diameter, was supplied by *Nachmann S.r.l.* (Milan, Italy). Ethanol and distilled water were purchased by *Sigma Aldrich*. All the materials were used as received.

2.2. Composite preparation

In this work, three preparation methods of the clay/active agent composites were tested: 1) wet impregnation, using an aqueous solution of thymol in which zeolite was suspended (Figure 1a); 2) semi-dry process, using ethanol as solvent for thymol (Figure 1b); 3) dry process, exploiting the melting of the active principle and its recrystallization in presence of the clay (Figure 1c).

In the first one, i.e., wet impregnation, an aqueous solution of thymol was prepared (using a thymol concentration equal to its solubility in water at 25 °C, 0.98 g/L). After complete thymol solubilization, ZEO4A (ratio zeolite/active principle equal to 1:1 w/w) was suspended under magnetic stirring (900 rpm for 30 min). Successively, the solid was

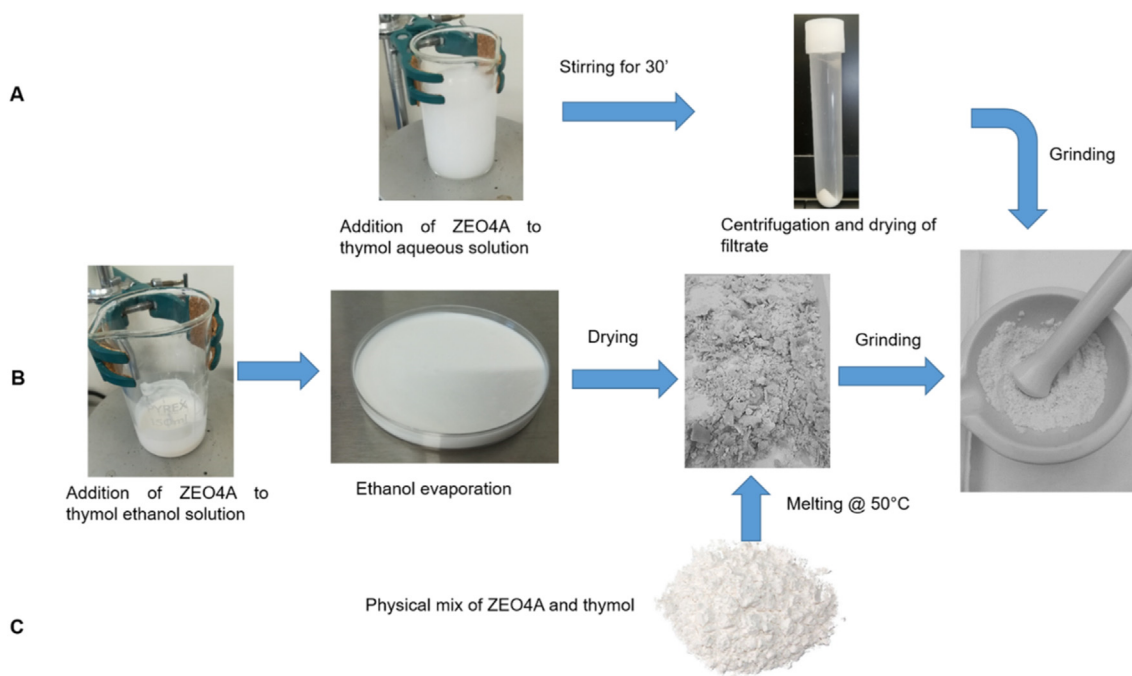


Figure 1. Preparation steps of the ZEO 4A/thymol composites: Panel A: wet procedure; panel B: semi-dry procedure; Panel C: dry procedure.

Table 1. Surface chemical composition of ZEO4A.

Element	At%
O1s	49.4
C1s	20.7
Si2p	8.7
Al2p	9.0
Na1s	12.2

centrifuged at a speed of 2250 rpm/min during 10 min and then dried at room temperature until constant weight. The ultimate hybrid composite was grinded in a mortar. In the second process, ethanol was used as solvent for thymol. Since thymol solubility in ethanol is very high (1000 g/L, at 25 °C), this process was called semi-dry, due to the very low solvent content (i.e., using an ethanol amount enough to solubilize the compound). Thymol was solubilized in ethanol and then ZEO4A (ratio zeolite/active principle equal to 1:1 w/w) was suspended under magnetic stirring (900 rpm for 30 min). The ethanol was allowed to evaporate at room temperature until constant weight of the composite. In the third process, the relatively low melting temperature of the active ingredient was exploited to perform a melting/crystallization cycle in the presence of the zeolite (i.e., a thermal treatment of thymol/zeolite physical mixture (ratio zeolite/active principle equal to 1:1 w/w), at 55 ± 2 °C for 10 min and the subsequent rapid solidification at room temperature). In this manner, recrystallization could be anyway influenced by the presence of the caged material. The ultimate step consisted in the grinding of the hybrid material.

2.3. Chemical-physical characterization of the composite

2.3.1. X-ray photoelectron spectroscopy (XPS)

XPS studies were carried out on ZEO4A clay by using a PHI 5000 VersaProbe II scanning microprobe, with a monochromatized AlK α X-ray radiation source (Physical Electronics, Chanhassen, MN). The samples were scanned in HP mode (sampled size $\sim 1400 \times 200 \mu\text{m}$), setting up an X-ray take-off angle of 45°. Wide scans and high-resolution regions were collected in FAT mode (pass energy 117.4 eV and 29.35 eV, respectively). The base pressure of the instrument was 10⁻⁹ mbar. The MultiPak software package (version 9.9.0.8) was exploited for data mining. The lower binding energy of C1s photo-peak (e.g., C1s hydrocarbon peak) was set at 284.8 eV as charge reference. Atomic percentages (At%) were calculated by means of normalized peak areas. Empirically derived sensitivity factors, in agreement with MultiPak library, enabled data comparison and peak areas normalization.

2.3.2. Fourier-transform infrared spectroscopy (FT-IR) in attenuated total reflectance mode (ATR)

FT-IR (ATR) was carried out by means of a Spectrum Two PE instrument (PerkinElmer Inc., Waltham, Massachusetts, USA) endowing the universal ATR accessory (UATR, Single Reflection Diamond/ZnSe). FT-IR/ATR spectra were recorded in the range between 400 and 4000 cm^{-1} (resolution 4 cm^{-1}).

2.3.3. X-ray diffraction analysis (XRD)

X-ray powder diffraction (XRD) profiles were acquired with an automatic X-ray diffractometer (Philips, now PANanalytical, United Kingdom) equipped with a Ni-filtered Cu-K α radiation. All the measurements were recorded from $2\theta = 5^\circ$ – 40° at a scan speed of 0.02°/s. The crystallite dimensions were extracted from the profiles using the Debye-Scherrer relation, according to which the average size of the crystallites, D , is related to β , the angular peak width at half maximum by the following Eq. (1):

$$D = \frac{K\lambda}{\beta \cos \theta} \quad (1)$$

where K is a dimensionless factor (approximated to 0.9), λ is the wavelength of the X-ray radiation used Cu-K α (1.5418 Å) and θ is the Bragg angle.

2.3.4. Thermal characterizations

Differential Scanning Calorimetry (DSC) analysis was performed using a Discovery DSC1-0145 (TA-Instrument New Castle, DE; USA). All the analyzed samples were heated from 15 to 70 °C (1st heating), then cooled down from 70 to -80 °C and finally heated up to 70 °C (2nd heating). The thermal scans were recorded at a scan speed of 5 °C/min under nitrogen flow in aluminum sealed pans. Thermograms were analyzed using the TA Universal Analysis software.

Thermo-Gravimetric Analysis (TGA) was performed on a PerkinElmer TGA-400 instrument (PerkinElmer Inc.), heating 5–10 mg of samples in air-saturated atmosphere, and setting the gas flow to 20 mL/min. The flow rate was set to 20 °C/min, heating from 30 to 800 °C. For each sample, thermograms (TG) with respective derivative (DTG) curves were recorded and analyzed with the TGA Pyris software.

2.3.5. Scanning electron microscopy/energy dispersive X-ray analysis (SEM/EDX)

The microstructural characterization of the composites was carried-out by a FESEM-EDX Carl Zeiss Sigma 300 VP electron microscope (Carl Zeiss Microscopy GmbH, Jena, Germany). The samples were fixed onto aluminum

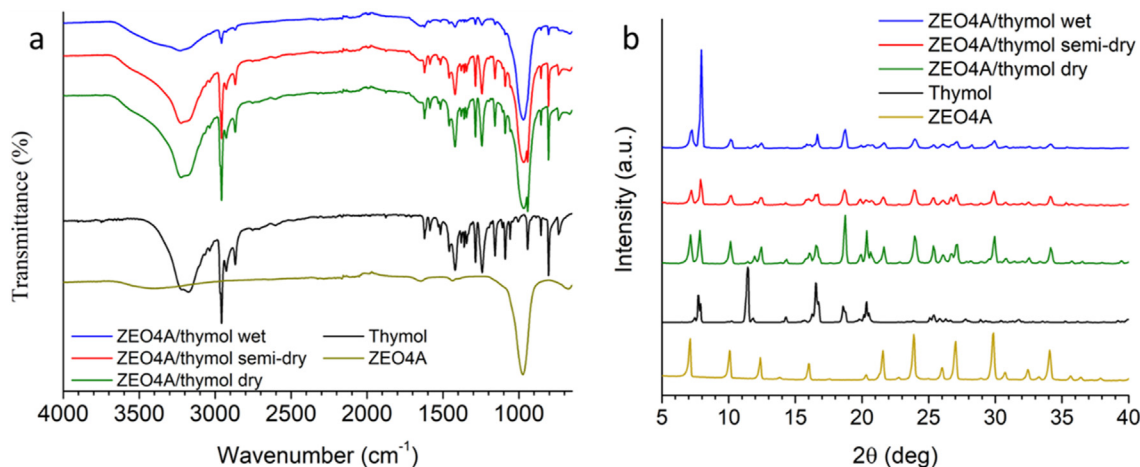


Figure 2. FT-IR/ATR (a) and XRD profiles (b) of pure thymol (black line), ZEO4A (dark yellow line), ZEO4A/thymol wet (blue line), ZEO4A/thymol semi-dry (red line) and ZEO4A/thymol dry (green line) formulations (a).

stubs with colloidal graphite and then sputtered with graphite (Sputter Quorum Q150 Quorum Technologies Ltd, East Sussex, UK). Beyond the morphological investigations, an energy dispersive X-ray (EDX) analysis was performed to gain insights into the elemental composition of the composites.

2.3.6. Specific surface area (SSA) and porosity determination

Brunauer, Emmett and Teller (B.E.T.) Specific Surface Area (SSA) of the samples was determined using an Autosorb IQ Chemi TCD instrument (Quantachrome Instruments, Boynton Beach, FL, USA) through adsorption-desorption N_2 isotherms at 77 K [28]. Powder samples were preventively outgassed at 45 °C for 120 min.

The Barrett, Joyner and Halenda (BJH) procedure was used to calculate, using the Kelvin equation, the pore surface area, volume, and average radius $Dv(r)$ [29]. All measurements were performed in triplicate.

2.3.7. Gas Chromatography - Mass Spectrometry (GC-MS)

GC-MS analyses were carried out by means of a Clarus 680 GC system coupled to the SQ 8T mass spectrometer (PerkinElmer Inc.), to determine thymol content within the prepared composites. Composite samples were incubated for 24 h in hexane at room temperature under static conditions, then the hexane containing the extracted thymol was diluted, filtered, and analyzed by the chromatographic method previously described in Pinto et al. [21]. Briefly, an ELITE 5-MS (PerkinElmer Inc.) column (0.30 m length \times 0.25 mm inner diameter \times 0.25 μ m full thickness) was eluted with helium at a constant pressure of 27 kPa. The external standard method was exploited to draw a thymol standard curve ($R^2 = 0.999$), allowing quantification. For each composite, the loading content and loading efficiency percentages (LC% and LE%, respectively) were calculated using Eqs. (2) and (3), respectively:

$$LC\% = (m_{\text{Loaded Thymol}} / m_{\text{composite}}) \times 100 \quad (2)$$

$$LE\% = (m_{\text{Loaded Thymol}} / m_{\text{Expected Thymol}}) \times 100 \quad (3)$$

where $m_{\text{Loaded Thymol}}$ and $m_{\text{Expected Thymol}}$ were the masses of thymol measured after the composite preparation and of thymol added during the preparation, respectively, while the $m_{\text{composite}}$ was the mass of the analyzed composite.

In addition, *in vitro* release tests were performed immersing 50 mg of the composites in 2 mL of physiological saline solution (NaCl 0.9% w/v) for 24 h. Then, thymol was extracted with hexane and determined by GC-MS analyses. Finally, storage stability tests were carried out incubating the composites at 25 °C up to 7 days in the dark. The residual content of thymol was assessed after 24 h, 48 h and 7 days.

2.4. In vitro antimicrobial assays

The evaluation of the antimicrobial activity of pure thymol and ZEO4A/thymol dry composite was carried out against *Candida albicans*

Table 2. Values of melting temperature (in °C), $T_{m, \text{onset}}$ melting temperature, T_m , onset glass transition temperature, T_g , and cold crystallization temperature, T_{cc} , extracted from the 1st and 2nd heating thermograms.

Sample	1st heating		2nd heating				
	$T_{m, \text{onset}}$	T_m	T_g	T_{cc}	$T_{m, \text{onset}}$	T_m	$T_{m, 2}$
Thymol	50.5	51.5	-	-	50.5	51.6	-
ZEO4A/thymol wet	47.4	49.8	-58.4	-31.5	47.4	49.5	51.0
ZEO4A/thymol semi-dry	49.2	49.9	-57.7	-31.0	47.5	49.5	51.1
ZEO4A/thymol dry	49.5	49.9	-57.7	-31.1	47.3	49.4	51.1

DSM 1386, *Escherichia coli* ATCC 34501, *Pseudomonas aeruginosa* DSM 939 and *Staphylococcus aureus* DSM 799 strains.

Microbial targets were routinely grown at 37 °C in Brain Heart Infusion (BHI) broth or Potato Dextrose broth (PDB) for bacteria and *Candida* strains, respectively. Before each assay, microbial suspensions were diluted to optical density of $OD_{600\text{nm}} = 0.30 \pm 0.05$.

Antimicrobial activity of thymol was initially evaluated by disk diffusion assay, as previously reported [30, 31]. Sterile cellulose blank disks (Oxoid, Thermo Fischer Scientific Inc. USA) were loaded with 20 μ L thymol solution (80–2.5 μ g/ μ L), or 100% hexane as negative control sample. Inoculated Petri dishes were stored for about one hour at 4 °C and then incubated at 37 °C for 24 h. At the end of incubation, the area of inhibition zones (mm^2) was measured by image analysis, as previously reported [21]. Furthermore, the Minimum Inhibitory Concentration (MIC) and the Minimum Bactericidal Concentration (MBC) of thymol were defined by microdilution method [32], in ISO sensitest broth (Oxoid, Thermo Fischer Scientific Inc.) [33]. After 24 h incubation at 37 °C, microbial growth was evaluated spectrophotometrically (Varioskan Flash, Thermo Fischer Inc.). The lowest thymol concentration inhibiting microbial growth (absorbance value lower than 0.05 after broth blanking) was recorded as the MIC. To assess the occurrence of viable cells, 50 μ L of broth from wells without microbial growth were inoculated in 5 mL of fresh broths defining the MBC when no visible growth was found after 24 h of incubation at 37 °C.

Finally, the antimicrobial activity of ZEO4A/thymol dry composite and pure thymol was compared through broth assay. Briefly, 100 μ L of fresh microbial cell suspension, standardized as above, was used to inoculate 10 mL of ISO-sensitest broth. Broth was supplemented with thymol at 11.25 mg/mL (75 mM), previously solubilized in absolute ethanol, or 22.50 mg/mL of ZEO4A/thymol dry composite (loading content close to 50% thymol). Inoculated broth and inoculated broth supplemented with ZEO4A, both at the same final ethanol concentration employed for thymol solution preparation, were used as negative control samples. After 24 h of incubation at 37 °C, all samples were diluted in sterile saline solution and plated on Plate Count Agar (PCA, Biolife

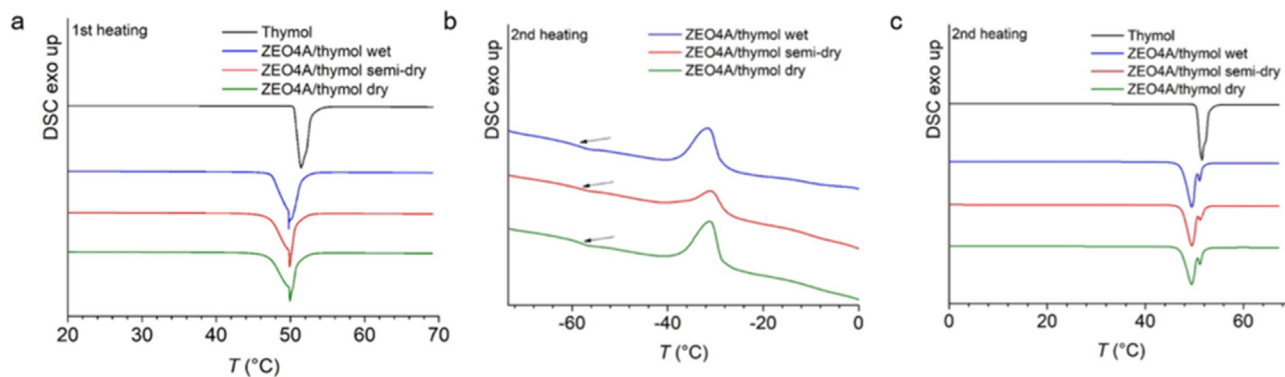


Figure 3. Thermograms of the first (a) and second heating (for sake of clarity, the thermograms are divided into two graphs: (b) from -80 to 0 °C and (c) from 0 to 70 °C) of pure thymol (black line), ZEO4A-thymol wet (blue line), ZEO4A-thymol semi-dry (red line) and ZEO4A-thymol dry (green line). The first heating was recorded from 15 to 70 °C at 5 °C/min, while the second one was recorded from -80 to 70 °C at 5 °C/min.

Italiana Srl, Milan, Italy) or Potato Dextrose Agar (PDA, *Biolife Italiana Srl.*) for the enumeration of survived bacteria and yeast cells, respectively. Both culture media were incubated for 24 h at 37 °C. Viable cell load was expressed as log cfu/mL.

2.5. Statistical analyses

Prism software (GraphPad, CA, USA) version 9.1.0 was exploited to perform statistical analyses. Storage stability as well as microbiological data were analyzed by means of one- or two-way ANOVA and Tukey HSD *post hoc* test. Statistical significance was set at $p < 0.05$.

3. Results and discussion

3.1. Chemical-physical and thermal characterization

3.1.1. XPS characterization of the clay

ZEO4A chemical composition was assessed by XPS analysis, as reported in Table 1. The theoretical chemical structure of ZEO4A was $\text{Na}_{12}[(\text{AlO}_2)_{12}(\text{SiO}_2)_{12}]x\text{nH}_2\text{O}$. The sodium ions can easily be exchanged by potassium, calcium, or many other metal ions. As observed by the elements detected on the surface, the sample was pure Na-zeolite. The calculated Si/Al ratio was equal to 0.97/1, as expected for an A-type zeolite. The binding energies of the Si2p and Al2p signals were 101.9 eV and 74.0 eV, respectively. These binding energies are typical of Al and Si present in the natural zeolite framework [34].

3.1.2. FT-IR/ATR analysis of the composites

The zeolite/thymol formulations were analyzed by means of FT-IR/ATR. The ATR spectra are reported, together with ZEO4A and thymol feed materials, in Figure 2a.

Thymol showed a band at about 3200 cm^{-1} , corresponding to phenolic O–H stretching involved in H bonds. The stretching of C–H fell in the $3000\text{--}2850\text{ cm}^{-1}$. The C=C stretching (1622 cm^{-1}), –OH bending (1360 cm^{-1}) and C–O stretching (1242 cm^{-1}) were typical of phenolic groups of thymol [35]. Moreover, out of plane vibrations (wagging) of aromatic C–H of thymol fell at 805 cm^{-1} [36]. In the spectrum of zeolite, the Si–O–Si or Si–O–Al vibrations in tetrahedra or alumino- and silico-oxygen bridges produced a strong adsorption band at around 976 cm^{-1} [37]. The bands at 3395 (i.e., –OH stretching) and 1644 cm^{-1} (i.e., –OH bending) could be ascribed to the adsorbed water [38]. The peak at 555 cm^{-1} could be assigned to the external vibration of double four-rings [39]. As far as the hybrid composites are concerned, no significant variations in the thymol and zeolite IR spectra were detected, indicating that

the inorganic support hosted the active principle without establishing chemical interactions with it, as already observed in the composites of Dikić et al., obtained by SSI [27]. Semi-dry and dry preparations revealed a much higher thymol loading than in the wet formulation. Finally, the wet procedure revealed a high water absorbed content and/or an extended H-bonded network (by the presence of a broadened band of OH stretching).

3.1.3. XRD analysis

X-ray diffraction patterns of thymol, ZEO4A and the three composites were reported in Figure 2b.

The zeolite, in accordance with literature data, showed narrow characteristic peaks, typical of the Lynde Type A zeolites with the cubic crystal system (spatial group $Fm\bar{3}c$), at $2\theta = 7.20^\circ, 12.4^\circ, 16.1^\circ, 20.4^\circ, 21.6^\circ, 26.1^\circ, 27.1^\circ, 30.0^\circ, 30.9^\circ, 32.5^\circ, \text{ and } 34.2^\circ$, corresponding respectively to *hkl* planes (200), (220), (222), (420), (440), (600), (622), (640), (642), (644), (660), (840) and (664) [40]. The positions of the zeolite reflections remained unchanged for all the composites, indicating that the zeolite structure was unaltered. The thymol diffraction pattern (Figure 2b, black curve) shows the crystalline nature of this compound. The peaks positions at $2\theta = 7.7^\circ, 11.4^\circ, 16.5^\circ, 18.6^\circ$ and 20.4° for thymol are in agreement with the structure solved by Thozet and Perrin [41].

Observing the diffraction patterns in Figure 2b, beside the reflection of the zeolites, crystalline peaks addressable to the thymol were observed also in the composites and resulted the same for the three composites. However, the relative intensities of the peaks were different with respect to the relative intensities of the thymol crystallized in absence of the zeolite. This suggests that the zeolite influenced the re-crystallization of the organic compound, inducing probably a preferential orientation. However, despite of the method used to prepare the composites (wet, semi-dry and dry), the thymol crystallized in the same form. The sizes of the thymol crystallites were evaluated analyzing the most intense peak at $2\theta = 7.8^\circ$. The thymol in the composites is characterized by greater values of the average size of crystallites with respect to values obtained in absences of zeolite for pure thymol, which resulted equal to 26.6 nm. Moreover, the size of crystallites was in the following order: wet > semi-dry > dry (i.e., 41.9, 34.6 and 33.2 nm for wet, semi-dry and dry formulations). This feature could be related to the fact that the crystallization of thymol was very fast in the dry process, intermediate in the semi-dry and slow in the wet one.

3.1.4. Thermal characterization of the composites

Thermal analyses performed by DSC allowed us to clarify the nature of the thymol contained in the composites, along with X-ray diffraction

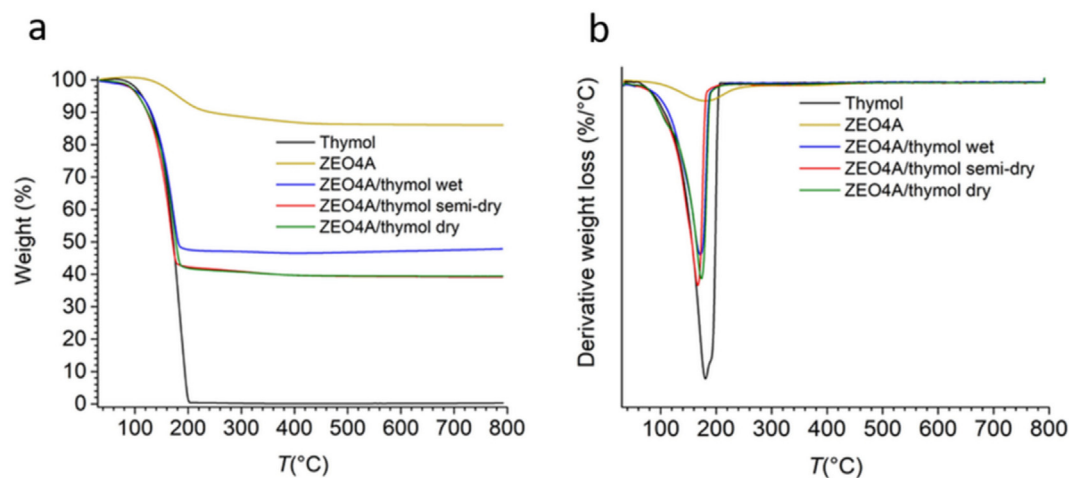


Figure 4. TGA (a) and derivative TGA (b) of Zeolite (dark yellow line), thymol (black line), ZEO4A/thymol wet (blue line), ZEO4A/thymol semi-dry (red line) and ZEO4A/thymol dry (green line) formulations.

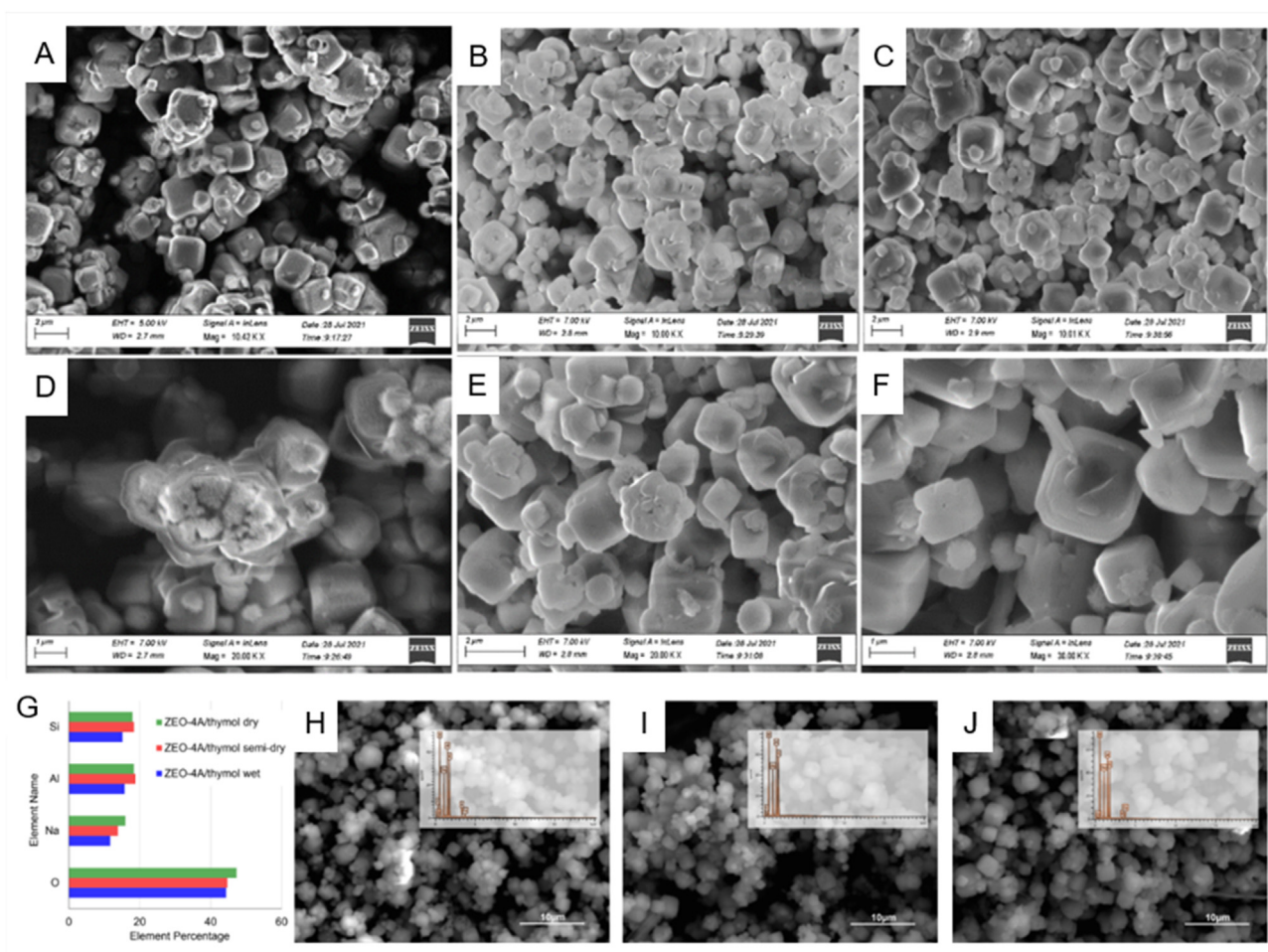


Figure 5. SEM characterizations of thymol-loaded ZEO4A composites. ZEO4A-Thymol wet (A, D), ZEO4A-Thymol semi-dry (B, E) and ZEO4A-Thymol dry (C, F). SEM-EDX characterizations of thymol-loaded ZEO4A composites. Elemental compositions (G), SEM images and EDX spectra of ZEO4A-Thymol wet (H) ZEO4A-Thymol semi-dry (I) and ZEO4A-Thymol dry (J).

results. The first heating from 15 to 70 °C was reported in Figure 3a. The ZEO4A/thymol composites exhibited a broad melting peak centered at the melting temperature, T_m , of ~49.9 °C, slightly lower than the T_m of pure thymol (51.5 °C). The broadness of the melting peak can be explained by the presence of different populations of crystals with different dimensions. This observation was consistent with the average size of the crystalline domains, extracted from X-ray diffraction profiles, which is bigger in the ZEO4A/thymol composites. Moreover, the melting process of the thymol in the composites was anticipated compared with the melting of pure thymol crystals, as demonstrated by the values of the onset temperatures, $T_{m,onset}$, reported in Table 2.

After the first heating, the samples were cooled down from 70 to -80 °C, allowing the re-crystallization under controlled conditions. Then, a successive heating (second heating) from -80 to 70 °C was recorded (Figures 3b and c).

It was observed that, in the composites, a small fraction of thymol was still amorphous, while, for the pure thymol, the amorphous phase was

not detected, meaning that all the thymol was present as crystalline. The amorphous fraction in ZEO4A/thymol samples showed a glass transition temperature, T_g , of ~-57-58 °C with slight differences between the three preparations. In details, the small shift of T_g at lower temperature for ZEO4A/thymol wet, in comparison with the dry and semi-dry formulation, could be due to the presence of molecules of water. The excess of water, derived from the casting procedure and confirmed by ATR analysis, can partially reduce the mobility of the amorphous phase because of H-bonding interactions between water and thymol molecules. The glass transition was followed by an exothermic event, occurring in all the ZEO4A/thymol samples. This event can be addressed to the cold crystallization of the amorphous phase, a phenomenon well known for polymers but still unexplored for small molecules. The temperature of cold crystallization, T_{cc} , lies at ~-31 °C for all the formulations. Our results are in good accordance with data reported by Pochivalov et al., which studied low density polyethylene-thymol systems, using a similar approach [42]. Finally, heating-up the samples to 70 °C, the melting of

Table 3. B.E.T. SSA, pore surface area, pore volume and pore radius (Dv(r)) of Zeo4A and ZEO 4A/thymol composites. All values differences were statistically significant according to ANOVA test (p-value 0.02).

Sample	B.E.T. SSA (m ² /g)	Pore surface area (m ² /g)	Pore volume (cc/g)	Dv(r) (Å)
ZEO4A	0.4 ± 0.1	0.4 ± 0.1	0.004 ± 0.001	17.5 ± 0.1
ZEO4A/thymol wet	1.7 ± 0.2	1.5 ± 0.2	0.012 ± 0.001	17.5 ± 0.8
ZEO4A/thymol semi-dry	2.2 ± 0.1	2.8 ± 0.1	0.014 ± 0.001	17.4 ± 0.8
ZEO4A/thymol dry	2.6 ± 0.2	3.2 ± 0.1	0.016 ± 0.001	18.3 ± 0.8

Table 4. Loading content (LC%) and Loading efficiency (LE%) of ZEO 4A/thymol composites assessed by GC-MS.

Sample	LC%	LE%
ZEO 4A/thymol wet	12.1 ± 0.8	24.2 ± 1.6
ZEO 4A/thymol semi-dry	46.3 ± 1.3	93 ± 3
ZEO 4A/thymol dry	49.8 ± 1.6	99.6 ± 1.2

the thymol was observed. As detected in the 1st heating, the melting of thymol crystals, during the 2nd heating, started at lower onset, $T_{m,onset}$, temperature values of ~47.4 °C with respect to the crystals in the pure thymol sample, which exhibited a higher $T_{m,onset}$ of ~50.5 °C. The pure thymol showed a single peak at $T_m = 51.6$ °C, otherwise the composites were characterized by an endotherm with two peaks not resolved. The main peak was centered at 49.5 °C while the less abundant peak was centered at $T_{m,2} = 51.1$ °C (see Table 2). According to the melting temperature values, the melting at $T_{m,2}$ can be due to the melting of a population of crystals more like the bulk crystals formed in absence of zeolite structure.

The thermograms and derivative thermograms relatives to thymol, ZEO4A and the wet, semi-dry and dry composites are reported in Figure 4a and b, respectively.

The thermogram of thymol showed one-step thermal degradation pattern, with the peak at 183 °C and the onset temperature at about 100 °C. The weight loss reached the 100% within 233 °C (i.e., the boiling point of thymol [43]). As far as ZEO4A sample is concerned, the first stage was relevant to desorption of physically adsorbed water or other volatiles within the zeolite cages (peak at 180 °C), equal to the 10.7% of the total sample weight. Successively, a second event (peak at 344 °C) was observed, corresponding to 3.4% of the weight of the sample, probably associated to the water loss from hydration complexes formed with exchangeable cations [44].

The ZEO4A/thymol hybrid prepared by wet process showed a degradation stage centered at about 177 °C (weight loss equal to 50.2%). On the other hand, the decomposition step of thymol was evident both in semi-dry and dry formulations, but at 173 and 161 °C, respectively (with weight losses equal to 59.9% and 62.5%, respectively). This reduced thermal stability of thymol entrapped in the zeolite can be related to a partial loss of crystallinity or formation of less stable crystals population, as also evidenced by DSC analysis.

3.1.5. Scanning electron microscopy/energy dispersive X-ray analysis (SEM/EDX)

SEM micrographs showed a very similar morphology of the three composites, consisting highly crystalline, chamfered-edged cubic structures of up to 2 μm size, typical of zeolite-A (Figure 5 A-F) [45], according to XRD experimental results. Large aggregation of the particles was observed in the composite obtained with the wet procedure (Figure 5 A, D), with lower

tendency in the semi-dry (Figure 5 B, E), probably due to solvent action. The best dispersion was found in the dry procedure (Figure 5 C, F).

EDX analyses confirmed the zeolite composition, mainly based on oxygen, silicon, aluminum, and sodium. Moreover, the Si/Al ratio for each sample was similar (Figure 5 G), achieving values between 0.96/1 and 0.98/1, in agreement with what observed by X-ray Photoelectron Spectroscopy (XPS) analysis (see Table 1).

3.1.6. Brunauer, Emmett and Teller (B.E.T.) analysis

Table 3 details the determined values of B.E.T. SSA [19], pore surface area, pore volume, and pore radius ($D_v(r)$), these last three estimated following the BJH method [20]. ZEO4A appears, according to literature [46], as a mesoporous material, with a pore radius and a pore surface area of about 17 Å and 0.4 m²/g, respectively. High values of B.E.T. SSA, as well as of pore surface area and volume, were obtained for ZEO4A/thymol composites, functional characteristics for a high zeolite-bacterial species interaction at the surface of the composite. Overall, these characteristics were affected by the treatments. Specifically, in comparison with wet and semi-dry samples, ZEO4A/thymol dry sample showed the highest values of B.E.T. SSA (2.6 ± 0.2 m²/g), in agreement with XRD experimental results and SEM observations, according to which the sample under examination was characterized by the smaller crystals (D 33.2 nm) with littler aggregation degree (see Figure 5). The highest values of pore surface area (3.2 ± 0.1 m²/g) and pore volume (0.016 ± 0.001 cc/g) of the considered composite, moreover, help to justify the specific surface area value just mentioned. In addition, in accordance with XRD and SEM results, ZEO4A/thymol wet showed also the lowest values of B.E.T. SSA (1.7 ± 0.2 m²/g), pore surface area (1.5 ± 0.2 m²/g) and volume (0.012 ± 0.001 cc/g). Intermediate porosity and SSA values characterized the ZEO4A/thymol semi-dry (B.E.T. SSA 2.2 ± 0.1 m²/g; pore surface area 2.8 ± 0.1 m²/g; pore volume 0.014 ± 0.001 m²/g).

No significant variation of pore radius dimension ($D_v(r)$) was observed, respect to ZEO4A, for each ZEO4A/thymol composite, suggesting that this parameter was not affected by the above-mentioned surface area values.

3.1.7. Quantification of thymol loading, release and storage stability by GC-MS

In Table 4, the loading content (LC%) and loading efficiency (LE%) relevant to the wet, semi-dry and dry processes, obtained by GC-MS analyses, are reported.

GC-MS analysis confirmed the low thymol content in the wet preparation, already qualitatively observed by FT-IR and TGA analyses. Furthermore, optimal loading efficiencies were achieved for both semi-dry and dry methods, although the last method resulted the best choice in view of potential industrial applications, since it was very fast (the preparation requires few minutes), avoided several steps (e.g., solvent removal, filtration, drying) that may reduce the amount of the active principle loaded in the composite.

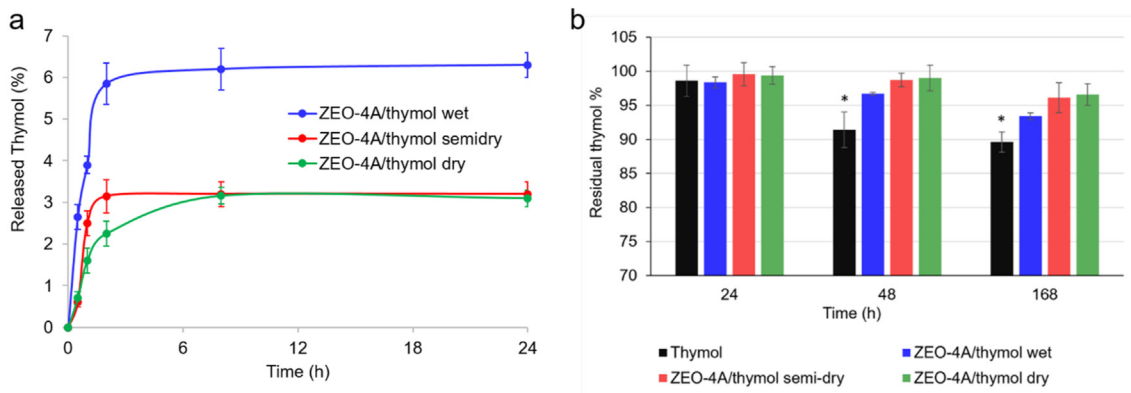


Figure 6. Percentage of thymol released in physiological solution over time (a); Residual thymol percentage with respect to the loading content, monitored at 25 °C; for each sampling time, asterisks indicate a statistically significant difference ($p < 0.05$) (b).

Table 5. Area of inhibition zones (mm²) of 20 μ L of thymol solutions against microbial pathogens after 24h incubation at 37 °C.

Concentration Thymol (μ g/ μ L)	<i>C. albicans</i> DSM 1386	<i>E. coli</i> ATCC 35401	<i>P. aeruginosa</i> DSM 939	<i>S. aureus</i> DSM 799
80	1020 \pm 110	660 \pm 30	138 \pm 7	>5000
40	590 \pm 16	490 \pm 30	108 \pm 15	950 \pm 30
20	205 \pm 7	164 \pm 13	73 \pm 6	371 \pm 30
10	106 \pm 10	75 \pm 9	71 \pm 11	260 \pm 20
5	0.00	34 \pm 11	37 \pm 6	0.00
2.5	0.00	0.00	0.00	0.00

Moreover, thymol release kinetics are reported in Figure 6a. Thymol release in NaCl 0.9% solution was quite low for all the prepared composites, as well as for pure thymol, whose water solubility is approximately 1 mg/mL [47]. Indeed, the percentage of thymol released respect to the total amount present in the three composites was equal to 6.3, 3.2 and 3.1% for wet, semidry and dry samples, respectively. It should be emphasized that, even if the percentage of thymol released appears to be higher in the wet than in the dry and semidry formulations, the absolute quantities of thymol released by the wet are much lower, due to the low LC % of the wet method. It could be hypothesized that thymol release is delayed by the presence of the caged inorganic structure, resulting in a more tortuous pathway, as already reported [48]. The release of essential oil compounds from zeolite is likely affected by steric effects. Indeed,

Dikić et al. (2021) [27] found a fast release of carvacrol and a slow release of thymol from clinoptinolite-zeolite based composites.

Percentage of thymol released in physiological solution over time (a); Residual thymol percentage with respect to the loading content, monitored at 25 °C; for each sampling time, asterisks indicate a statistically significant difference ($p < 0.05$) (b). Noteworthy, an antimicrobial system displaying low thymol release could be advantageous for several applications in personal care (i.e., skin contact products). Moreover, a high release could also be detrimental, causing environmental disposal issues [49].

In addition, storage tests were performed at 25 °C up to 7 days, to observe thymol concentration decay over time, comparing pure thymol stability with that of thymol in the composites (Figure 6b).

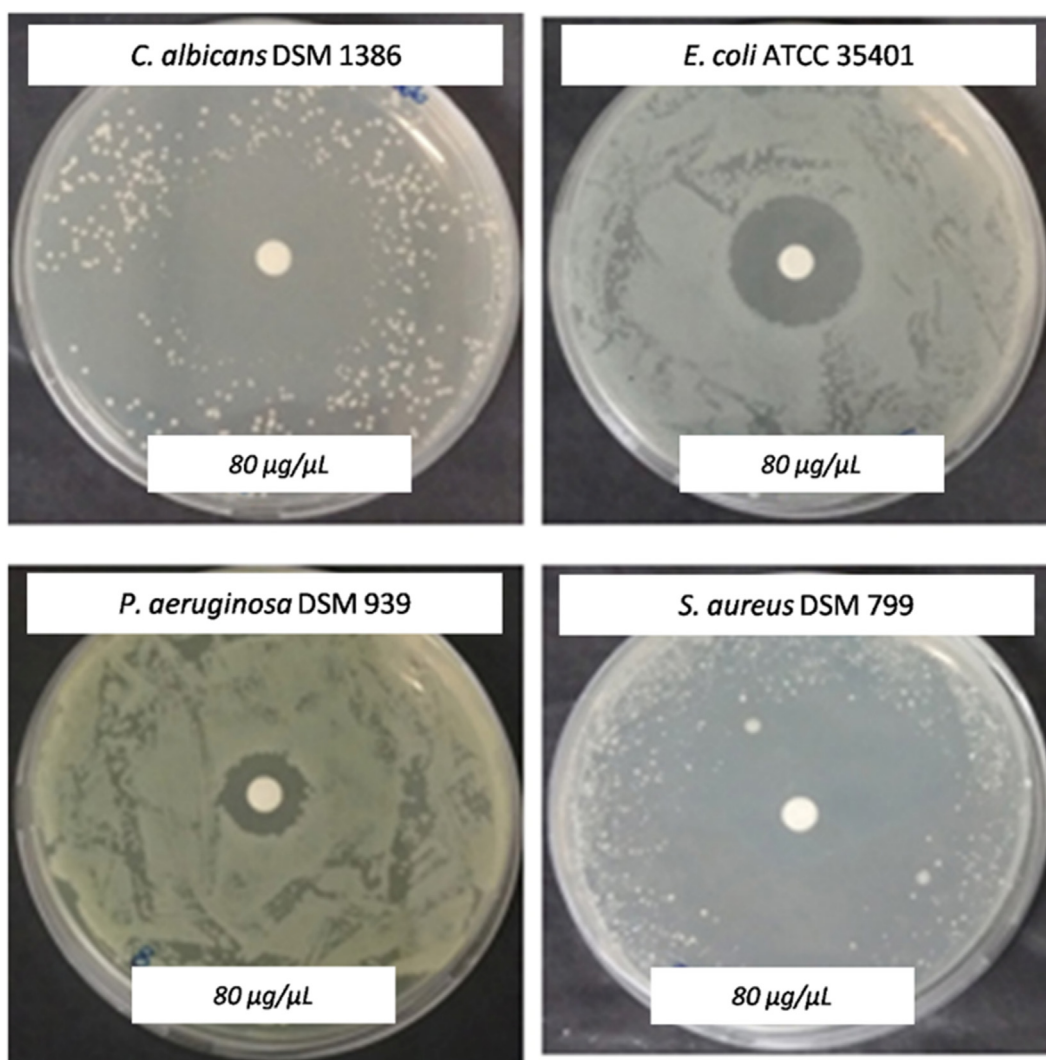
**Figure 7.** Inhibition zones (mm²) produced by thymol solution (20 μ L of the 80 μ g/ μ L solution) against *C. albicans* DSM 1386, *E. coli* ATCC 35401, *P. aeruginosa* DSM 939, and *S. aureus* DSM 799 after 24 h of incubation at 37 °C.

Table 6. Viable cell count (expressed in log cfu/mL) of target microbial strains after 24h contact (37 °C) with ZEO4A, thymol and ZEO4A/thymol dry.

	T0	Control	ZEO 4A	Thymol	ZEO4A/thymol dry
<i>C. albicans</i> DSM 1386	4.62 ± 0.12 ^a	6.72 ± 0.14 ^b	6.73 ± 0.17 ^b	nd ^c	nd ^c
<i>E. coli</i> ATCC 35401	5.93 ± 0.14 ^a	9.38 ± 0.12 ^b	9.4 ± 0.3 ^b	nd ^c	nd ^c
<i>P. aeruginosa</i> DSM 939	6.72 ± 0.14 ^a	9.3 ± 0.3 ^b	9.45 ± 0.19 ^b	5.9 ± 0.2 ^c	nd ^d
<i>S. aureus</i> DSM 799	5.61 ± 0.16 ^a	9.0 ± 0.2 ^b	8.5 ± 0.2 ^c	nd ^d	nd ^d

nd: not detected, limit of detection 2 log cfu/mL.

After 24 h at 25 °C, no differences in thymol content were observed between pure thymol and the composites. Conversely, after 48 h and 7 days, the three composites allowed a higher preservation of thymol content as compared to pure thymol ($p < 0.05$). No statistically significant differences were observed at each time point among the three formulations.

3.2. Antimicrobial assessment of thymol and ZEO4A/thymol dry composite

The first antimicrobial assay was carried out to assess the antimicrobial activity played by thymol against the four microbial pathogens (three bacteria and one yeast) considered in the present work, and potentially contaminating sanitary devices, mucous membranes, foods, and different surfaces. Thus, the inhibition halo surrounding a cellulose disk loaded with thymol solutions at different concentration was measured.

A good correlation between thymol concentration in the cellulose disk and area of inhibition was found after 24 h (Table 5). The blank disk loaded only with hexane did not produce any inhibition zone against the four strains herein assayed. Among microbial strains assayed, the less sensitive was *P. aeruginosa* DSM 939, whereas the most sensitive was *S. aureus* DSM 799.

In particular, the growth of *S. aureus* DSM 799 was inhibited almost up to the edge of the Petri dish (inhibition zone $>5000 \text{ mm}^2$), even though several small colonies grown separately each other far from the cellulose disk (Figure 7).

Then, MIC and MBC of thymol, prepared in absolute ethanol, and diluted in ISO-sensitest broth were measured. *C. albicans* DSM 1386 and *E. coli* ATCC 35401 showed MIC values of 2.5 mM whereas their MBCs were 2.50 and 5.00 mM, respectively. In accordance with results of disk diffusion assays, *P. aeruginosa* DSM 939 was found the most resistant strain to thymol treatment with MIC value $>20.00 \text{ mM}$, whereas *S. aureus* DSM 799 was the most sensitive with MIC of 1.25 mM and MBC of 5 mM.

To compare the antimicrobial activity of thymol and that of the ZEO4A/thymol hybrid composite prepared through the dry process, microbial cells were incubated at the same estimated thymol concentration of 75 mM enumerating the survivors after 24 h of contact at 37 °C. The estimated thymol concentration was three times higher than MIC values of moderate sensitive strains (*C. albicans* DSM 1386 and *E. coli* ATCC 35401) but lower than that related to *P. aeruginosa*. As shown in Table 6, all strains grew well in ISO-sensitest broth with or without ZEO4A.

In accordance with the results of MIC and MBC, the thymol concentration of 75 mM completely suppressed the viability of all strains, except *P. aeruginosa* DSM 939. This strain was still alive after 24 h of contact with thymol, showing a viable load close to that measured at the beginning of incubation. This result suggests a bacteriostatic effect of 75 mM thymol against *P. aeruginosa* DSM 939. However, viable *P. aeruginosa* DSM 939 cells were not found after incubation with the ZEO4A/thymol dry composite.

Usually, non-exchanged zeolites (Na-zeolites) did not show antibacterial activity against various bacteria [50, 51] even though Na-clinoptinolite resulted active against *Helicobacter pylori* [52] as well as commercial zeolite A showed antimicrobial activity against *Acinetobacter junii* and *Saccharomyces cerevisiae* in watery medium [53]. In this respect,

ZEO 4A did not show antibacterial activity against different strains (Table 6), even though slightly decreased the viability of *S. aureus* DSM 799 after 24h of incubation.

Even though thymol antimicrobial action is mainly elicited by contact-killing mechanisms such as bacterial membrane disruption [54], the thymol concentration released from ZEO4A/thymol dry composite in physiological solution (ca. 2.6 mM), excludes this antimicrobial mechanism for *P. aeruginosa* DSM 939. However, similar results were already reported. Recently, palygorskite loaded with thymol showed antibacterial activity against *E. coli* and *S. aureus* higher than pure compound, probably due to enhanced hydrophilicity and dispersion of these antimicrobials conveyed through clays [55]. These results were confirmed in clinoptinolite-zeolite loaded with thymol or carvacrol composites obtained by SSI, which showed that the bactericidal activity against *E. coli* and *S. aureus* in water media could not be ascribed only to the release of monoterpene compounds, but also properties of the composite material [27]. Monoterpene compounds such as thymol and carvacrol can be adsorbed on the external Na^+ -montmorillonite surface through hydrogen bonds between OH- groups of the essential oil compounds and OH-groups of the clay [56]. A similar interaction could occur between thymol and ZEO4A interfaces, suggesting a potential role in the antimicrobial activity of our composite, in particular against *Pseudomonas aeruginosa*.

In absence of specific assays, we can postulate that the antimicrobial activity found was the result of peculiar new properties of the ZEO4A/thymol dry composite, such as the highest values of B.E.T. SSA, pore surface area, and pore volume. Further research is necessary to shed light on the enhanced antibacterial action of ZEO4A/thymol dry composite compared to pure thymol against *P. aeruginosa* DSM 939.

Means followed by different lowercase letters are significantly different within rows ($P < 0.05$) after one-way ANOVA followed by post-hoc Tukey Test.

4. Conclusions

In this work, the effect of thymol incorporation in zeolite network by three different procedures on the chemical-physical, thermal, and structural properties was investigated. The dry method proved to be the most promising for the development of bioactive antimicrobial composites, being a fast, highly efficient, eco-sustainable and scalable process. The dry composite was easy to be prepared, with excellent yields. Indeed, this solvent-free procedure allowed us to maximize the loading efficiency of thymol and to obtain a fast thymol crystallization with the lowest crystallites size. Moreover, it reduced thymol volatility, representing an interesting solution to minimize the odor impact of the final formulation, which could hinder some applications.

In addition, ZEO4A/thymol dry formulation demonstrated strong antibacterial effect against all pathogens involved in different urogenital disorders, probably also to the high SSA and pore surface area of this composite, which results in a large contact surface and, therefore, in a good interaction between the surface of the composite and the bacterial target. In the case of *P. aeruginosa* DSM 939, ZEO4A/thymol dry formulation showed enhanced antibacterial action in comparison to the same concentration of pure thymol. The low thymol release into the environment, its improved physical stability, and the antimicrobial activity of the

composite surfaces, are the premises for the inclusion of ZEO4A/thymol dry powder in different disposable products, such as detergents, paints, waxes, lotions, gels, emulsions, bleaching agents, disinfectants, tooth-pastes, deodorants, perfumes, sanitary devices etc., addressed to preserve hygienic conditions of external mucosae.

Declarations

Author contribution statement

Stefania Cometa: Conceived and designed the experiments; Performed the experiments; Analyzed and interpreted the data; Wrote the paper.

Maria A. Bonifacio, Loris Pinto: Performed the experiments; Analyzed and interpreted the data; Wrote the paper.

Annalisa Bellissimo, Andrea Petrella, Nicoletta De Vietro: Performed the experiments; Analyzed and interpreted the data; Contributed reagents, materials, analysis tools or data; Wrote the paper.

Giuseppe Iannaccone: Conceived and designed the experiments; Contributed reagents, materials, analysis tools or data; Wrote the paper.

Federico Baruzzi, Elvira De Giglio: Conceived and designed the experiments; Analyzed and interpreted the data; Contributed reagents, materials, analysis tools or data; Wrote the paper.

Funding statement

This work was supported by the Italian Ministry of Economic Development (Dec. MISE n. F/050056/01-02/X32, August 9th, 2017, Horizon 2014-2020 PON I&C), in the framework of the project "Da risorse naturali a materiali innovativi: compositi multifunzionali per applicazioni nel settore igienico-sanitario (GreenMAT)".

Data availability statement

Data will be made available on request.

Declaration of interests statement

The authors declare no conflict of interest.

Additional information

No additional information is available for this paper.

Acknowledgements

Authors greatly acknowledge Plastik Textile S.p.A. (Albano Sant'Alessandro, Bergamo, Italy), in the person of Mr Gianangelo Cattaneo, Dr. Laura Cattaneo and Dr. Luca Marinucci. Prof. Odda Ruiz de Ballesteros and Dr. Francesca Gargiulo are kindly acknowledged for providing the equipment and technical support for XRD analysis.

References

- E. Jacopin, S. Lehtinen, F. Débarre, J.R. Blanquart, Factors favouring the evolution of multidrug resistance in bacteria, *Soc. Interface* 17 (2020) 1.
- G.V. Vimbela, S.M. Ngo, C. Frazee, L. Yang, D.A. Stout, Antibacterial properties and toxicity from metallic nanomaterials, *Int. J. Nanomed.* 12 (2017) 3941.
- D.S. Alviano, C.S. Alviano, Plant extracts: search for new alternatives to treat microbial diseases, *Curr. Pharm. Biotechnol.* 10 (2009) 106.
- B. Salehi, A.P. Mishra, I. Shukla, M. Sharifi-Rad, M.D.M. Contreras, A. Segura-Carretero, H. Fathi, N.N. Nasrabadi, F. Kobardard, J. Sharifi-Rad, Thymol, thyme, and other plant sources: Health and potential uses, *Phytother. Res.* 32 (2018) 1688.
- Y. Li, J.M. Wen, C.J. Du, S.M. Hu, J.X. Chen, S.G. Zhang, N. Zhang, F. Gao, S.-J. Li, X.-W. Mao, H. Miyamoto, K.F. Ding, Thymol inhibits bladder cancer cell proliferation via inducing cell cycle arrest and apoptosis, *Biochem. Biophys. Res. Commun.* 491 (2017) 30.
- S. Tariq, S. Wani, W. Rasool, K. Shafi, M.A. Bhat, A. Prabhakar, A.H. Shalla, M.A. Rather, A comprehensive review of the antibacterial, antifungal and antiviral potential of essential oils and their chemical constituents against drug-resistant microbial pathogens, *Microb. Pathog.* 134 (2019) 103580.
- P.C. Braga, M. Dal Sasso, M. Culici, T. Bianchi, L. Bordoni, L. Marabini, Anti-inflammatory activity of thymol: inhibitory effect on the release of human neutrophil elastase, *Pharmacology* 77 (2006) 130.
- S. Yildiz, S. Turan, M. Kiralan, M.F. Ramadan, Evaluation of the Anticancer Activity of Phytomolecules Conjugated Gold Nanoparticles Synthesized by Aqueous Extracts of *Zingiber officinale* (Ginger) and *Nigella sativa* L. Seeds (Black Cumin), *J. Food Meas. Charact.* 15 (2020) 621.
- Y.P. Bhalerao, S.J. Wagh, A Review on Newer Ocular Drug Delivery Systems with an Emphasis on Glaucoma, *Int. J. Pharm. Res.* 14 (2018) 114.
- I.M. Martins, S.N. Rodrigues, M.F. Barreiro, A.E. Rodrigues, Polylactide-Based Thyme Oil Microcapsules Production: Evaluation of Surfactants, *Ind. Eng. Chem. Res.* 51 (2012) 11565.
- C.C. Liolios, O. Gortzi, S. Lalas, J. Tsaknis, I. Chinou, Liposomal incorporation of carvacrol and thymol isolated from the essential oil of *Origanum dictamnus* L. and in vitro antimicrobial activity, *Food Chem* 112 (2009) 77.
- K.K. Li, S.W. Yin, X.Q. Yang, C.H. Tang, Z.H. Wei, Fabrication and characterization of novel antimicrobial films derived from thymol-loaded zein-sodium caseinate (SC) nanoparticles. *J. Agric. Food Chem.* 60 (2012) 11592.
- J. Li, J.W. Chang, M. Saenger, A. Deering, Thymol nanoemulsions formed via spontaneous emulsification: Physical and antimicrobial properties, *Food Chem* 232 (2017) 191.
- L. Pinto, M.A. Bonifacio, E. De Giglio, E. Santovito, S. Cometa, A. Bevilacqua, F. Baruzzi, Biopolymer hybrid materials: Development, characterization, and food packaging applications, *Food Packag. Shelf Life* 28 (2021) 100676.
- F. García-Villén, E. Carazo, A. Borrego-Sánchez, R. Sánchez-Espejo, P. Cerezo, C. Viseras, C. Aguzzi, in: M. Mercurio, B. Sarkar, A. Langella (Eds.), *Modified clay and Zeolite Nanocomposite Materials*, Elsevier, Amsterdam, 2018. Chapter 6.
- J.N. Saucedo-Zúñiga, S. Sánchez-Valdes, E. Ramírez-Vargas, L. Guillen, L.F. Ramos-deValle, A. Graciano-Verdugo, J.A. Uribe-Calderón, M. Valera-Zaragoza, T. Lozano-Ramírez, J.A. Rodríguez-González, J.J. Borjas-Ramos, J.D. Zuluaga-Parra, Controlled release of essential oils using laminar nanoclay and porous halloysite / essential oil composites in a multilayer film reservoir, *Micropor. Mesopor. Mat.* 316 (2021) 110882.
- M.G. Nguemtchouin, M.B. Ngassoum, P. Chalié, R. Kamga, L.S. Ngamo, M. Cretin, *Ocimum gratissimum* essential oil and modified montmorillonite clay, a means of controlling insect pests in stored products, *J. Stored Prod. Res.* 52 (2013) 57.
- S. Appavoo, A. Bhattacharya, S.G. Dastidar, M.T. Saji, U.S. Patent, 2017. <https://patents.google.com/patent/US975685B2/en>.
- S. Gueu, V.E. Tia, D. Bartier, O. Barres, F.D. Soro, Adsorption of *Lippia multiflora* essential oil on two surfactant-modified clays: qualitative approach, *Clay Miner* 55 (2020) 219.
- A. Giannakas, I. Tsagkalias, D.S. Achilias, A. Ladavos, A novel method for the preparation of inorganic and organo-modified montmorillonite essential oil hybrids, *Appl. Clay Sci.* 146 (2017) 362.
- L. Pinto, M. Cefola, M.A. Bonifacio, S. Cometa, C. Bocchino, B. Pace, E. De Giglio, M. Palumbo, A. Sada, A.F. Logrieco, F. Baruzzi, Effect of red thyme oil (*Thymus vulgaris* L.) vapours on fungal decay, quality parameters and shelf-life of oranges during cold storage, *Food Chem* 336 (2021) 127590.
- K. Tyan, A. Levin, A. Avalos-Pacheco, D. Plana, E.A. Rand, H. Yang, L.E. Maliszewski, L.A. Chylek, L. Atta, M.A. Tye, M.M. Carmack, N.S. Oglesby, S. Burgin, S.H. Yu, N.R. LeBoeuf, J.M. Kemp, Considerations for the Selection and Use of Disinfectants Against SARS-CoV-2 in a Health Care Setting, *Open Forum Infect. Dis.* 7 (2020) 1.
- L. Pinto, M.A. Bonifacio, E. De Giglio, S. Cometa, A.F. Logrieco, F. Baruzzi, Unravelling the Antifungal Effect of Red Thyme Oil (*Thymus vulgaris* L.) Compounds in Vapor Phase, *Molecules* 25 (2020) 4761.
- Y. Li, L. Li, J. Yu, Applications of Zeolites in Sustainable Chemistry, *Chem* 3 (2017) 928.
- S. Demirci, Z. Ustaoglu, G.A. Yilmazer, F. Sahin, N. Baç, Antimicrobial properties of zeolite-X and zeolite-A ion-exchanged with silver, copper, and zinc against a broad range of microorganisms, *Appl. Biochem. Biotechnol.* 172 (2014) 1652.
- M.M. Salim, N.A.N.N. Malek, N.I.A. Ramli, S.A.M. Hanim, S. Hamdan, Antibacterial activity of CTAB-modified zeolite NaY with different CTAB loading, *Mal. J. Fund. Appl. Sci.* 10 (2014) 129.
- J. Dikić, I. Lukić, J. Pajnik, J. Pavlović, J. Hrenović, N. Rajić, Antibacterial activity of thymol/carvacrol and clinoptilolite composites prepared by supercritical solvent impregnation, *J. Porous Mater.* 28 (2021) 1557.
- S. Brunauer, P.H. Emmett, E. Teller, Adsorption of Gases in Multimolecular Layers, *J. Am. Chem. Soc.* 60 (1938) 309.
- E.P. Barrett, L.G. Joyner, P.P. Halenda, The Determination of Pore Volume and Area Distributions in Porous Substances. I. Computations from Nitrogen Isotherms, *J. Am. Chem. Soc.* 73 (1951) 373.
- A.R. Ahameethunisa, W. Hopper, Antibacterial activity of *Artemisia nilagirica* leaf extracts against clinical and phytopathogenic bacteria, *BMC Complement. Altern. Med.* 10 (2010) 6.
- P.A. Wayne, NCCLS, National Committee for Clinical Laboratory Standards (NNCLS Publications), Wayne Penn., sixth ed., 1997.
- P.A. Wayne, Twenty-Fifth Informational Supplement, NCCLS, National Committee for Clinical Laboratory Standards (NNCLS publications), Wayne Penn., 2015.
- L.M. Koeth, A. King, H. Knight, J. May, L.A. Miller, I. Phillips, J.A. Poupard, Comparison of cation-adjusted Mueller–Hinton broth with Iso-Sensitest broth for the NNCLS broth microdilution method, *J. Antimicrob. Chemother.* 46 (2000) 369.
- X. Wang, C.A. Plackowski, A.V. Nguyen, X-ray photoelectron spectroscopic investigation into the surface effects of sulphuric acid treated natural zeolite, *Powder Technol* 295 (2016) 27.

- [35] A. Rukmani, S. Mahalingam, Inclusion of antibacterial agent thymol on β -cyclodextrin-grafted organic cotton, *J. Ind. Text.* 42 (2012) 132.
- [36] D. Markovic, S. Milovanovic, M. Radetic, B. Jokic, I. Zizovic, Impregnation of corona modified polypropylene non-woven material with thymol in supercritical carbon dioxide for antimicrobial application, *J. Supercrit. Fluids* 101 (2015) 215.
- [37] M.S. Boroglu, M.A. Gurkaynak, Fabrication and characterization of silica modified polyimide-zeolite mixed matrix membranes for gas separation properties, *Polym. Bull.* 66 (2011) 463.
- [38] S. Su, H. Ma, X. Chuan, Hydrothermal synthesis of zeolite A from K-feldspar and its crystallization mechanism, *Adv. Powder. Technol.* 27 (2016) 139.
- [39] P. Krongkrachang, P. Thungngern, P. Asawaworarit, N. Hounkanghang, A. Eiad-Ua, Synthesis of Zeolite Y from Kaolin via hydrothermal method, *Mater. Today: Proc.* 17 (2019) 1431.
- [40] J.J. Pluth, J.V. Smith, Accurate redetermination of crystal structure of dehydrated zeolite A. Absence of near zero coordination of sodium. Refinement of silicon, aluminum-ordered superstructure, *J. Am. Chem. Soc.* 102 (1980) 4704.
- [41] A. Thozet, M. Perrin, Structure of 2-isopropyl-5-methylphenol (thymol), *Acta Crystallogr. B: Struct. Sci. Cryst. Eng. Mater.* B36 (1980).
- [42] K.V. Pochivalov, A.V. Basko, T.N. Lebedeva, L.A. Antina, R.Y. Golovanov, V.V. Artemov, A.A. Ezhov, Y.V. Kudryavtsev, Thermal and optical studies on the compositions of low-density polyethylene with highly refined mineral oil, *Thermochim. Acta* 659 (2018) 113.
- [43] Y. Wu, Y. Luo, B. Zhou, L. Mei, Q. Wang, B. Zhang, Porous metal-organic framework (MOF) Carrier for incorporation of volatile antimicrobial essential oil, *Food Control* 98 (2019) 174.
- [44] S. Akbar, K. Dad, T.H. Shah, R. Shahnaz, Thermal studies of NaX zeolite with different degrees of cadmium exchange, *J. Chem. Soc. Pak.* 27 (2005) 456.
- [45] J.W. Park, K.H. Ahn, W.K. Lee, C.H. Lee, Crystallization properties of zeolite A synthesized from coal fly ash using a fusion/hydrothermal method, *Mol. Cryst. Liq. Cryst.* 687 (2019) 89.
- [46] J. Liang, Z. Liang, R. Zou, Y. Zhao, Heterogeneous Catalysis in Zeolites, Mesoporous Silica, and Metal-Organic Frameworks, *Advanced Mat* 29 (2017) 1701139.
- [47] M.J. O'Neil, P.E. Heckelman, P.H. Dobbelaar, K.J. Roman, C.M. Kenny, L.S. Karaffa, Royal Society of Chemistry, Cambridge, fifteenth ed., 2013.
- [48] V.H. Campos-Requena, B.L. Rivas, M.A. Pérez, C.R. Figueroa, E.A. Sanfuentes, The synergistic antimicrobial effect of carvacrol and thymol in clay/polymer nanocomposite films over strawberry gray mold, *LWT Food Sci. Technol.* 64 (2015) 390–396.
- [49] Chemical risk information platform (CHRIP), biodegradation and bioconcentration. https://www.nite.go.jp/en/chem/chrip/chrip_search/srhInput. (Accessed 20 January 2022).
- [50] P. Saint-Cricq, Y. Kamimura, K. Itabashi, A. Sugawara-Narutaki, A. Shimojima, T. Okubo, Antibacterial Activity of Silver-Loaded “Green Zeolites”, *Eur. J. Inorg. Chem.* 21 (2012) 3398.
- [51] T.J. Daou, T. Dos Santos, H. Nouali, L. Josien, L. Michelin, L. Pieuchot, P. Dutournie, Synthesis of FAU-Type Zeolite Membranes with Antimicrobial Activity, *Molecules* 25 (2020) 3414.
- [52] M. Farina, A. Brundu, M.C. Bonferoni, C. Juliano, G. Rassu, E. Gavini, G. Cerri, Antibacterial activity of Na-clinoptilolite against *Helicobacter pylori*: in-vitro tests, synergistic effect with amoxicillin and stability of the antibiotic formulated with the zeolite, *Micropor Mesopor Mat* 288 (2019) 109592.
- [53] J. Hrenović, D. Zeljezić, N. Kopjar, A. Sarpola, J. Bronić, L. Sekovanić, Antimicrobial activity of commercial zeolite A on *Acinetobacter junii* and *Saccharomyces cerevisiae*, *J. Hazard. Mater.* 183 (2010) 655.
- [54] K. Kachur, Z. Suntres, The antibacterial properties of phenolic isomers, carvacrol and thymol, *Crit. Rev. Food Sci. Nutr.* 60 (2020) 3042.
- [55] H. Zhong, B. Mu, P. Yan, Y. Jing, A. Hui, A. Wang, A comparative study on surface/interface mechanism and antibacterial properties of different hybrid materials prepared with essential oils active ingredients and palygorskite, *Colloids Surf. A Physicochem. Eng. Asp.* 618 (2021) 126455.
- [56] K. Essifi, A. Hammani, D. Berraouan, A. El Bachiri, M.L. Fauconnier, A. Tahani, Montmorillonite nanoclay based formulation for controlled and selective release of volatile essential oil compounds, *Mater. Chem. Phys.* 277 (2021) 125569.